frontiers | Frontiers in Physics

TYPE Original Research
PUBLISHED 22 August 2023
DOI 10.3389/fphy.2023.1241533

OPEN ACCESS

EDITED BY
Boyang Xue,
Qilu University of Technology, China

REVIEWED BY
Pavel Pořízka,
Brno University of Technology, Czechia
George Chan,
Berkeley Lab (DOE), United States

*CORRESPONDENCE
Jens Riedel,
jens.riedel@bam.de

RECEIVED 16 June 2023
ACCEPTED 17 July 2023
PUBLISHED 22 August 2023

CITATION
Riedel J, Hufgard J and You Y (2023), LIBS at high duty-cycles: effect of repetition rate and temporal width on the excitation laser pulses.
Front. Phys. 11:1241533.
doi: 10.3389/fphy.2023.1241533

LIBS at high duty-cycles: effect of repetition rate and temporal width on the excitation laser pulses

Jens Riedel *, Josefin Hufgard and Yi You

Bundesanstalt für Materialforschung und -prüfung (BAM), Berlin, Germany

Laser-induced breakdown spectroscopy (LIBS) is becoming a more mature technology every year with new variants such as laser ablation molecular isotopic spectrometry, reheating by various discharge techniques, and multiple pulse excitation schemes, in which sometimes lasers of different pulse lengths are used. However, lasers with inherent parameters like pulse length and repetition rate are still almost exclusively employed. Recent years have witnessed the advent of novel high-repetition-rate laser concepts for machining processes, like welding, milling, and engraving. Here, a comprehensive study of single-pulse LIBS spectra of a single aluminum target is presented to showcase the applicability of flexible high duty-cycle master oscillator power amplifier (MOPA) lasers. Although traditional flashlamp-pumped Fabry–Pérot lasers only permit a variation in the pulse energy and are operated at very low duty-cycles, MOPA lasers add repetition rate and pulse length as variable parameters. A thorough analysis of the temporal plasma behavior revealed the emission dynamic to closely match the excitation laser pulse pattern. An aluminum sample's spectral response was shown to be significantly impacted by variations in both rate and length. Although the spectral emission strength of the elemental lines of Al, Sr, and Ca all peaked at slightly different parameter settings, the strongest impact was found on the relative abundance of molecular AlO bands. Unlike in previous laser ablation molecular isotopic spectrometry (LAMIS) publications, the latter could be readily detected with a good intensity and well-resolved spectral features without any temporal gating of the detector. This finding, together with the fact that MOPA lasers are both inexpensive and dependable, makes for a promising combination for future studies including the detection of diatomic band structures.

KEYWORDS

laser-induced breakdown spectroscopy, plasma, master oscillator power amplifier, long pulse, aluminum, laser ablation molecular isotopic spectrometry

1 Introduction

In laser-induced breakdown spectroscopy (LIBS), all characteristic plasma properties, which eventually result in the analytical applicability and performance of the experiment, are dictated by the used laser-pulse features. In addition to its wavelength λ and the pulse energy E, the most influential properties of the output of a pulsed laser are pulse length τ and the repetition rate f_{rep}. A related parameter that is not usually considered is the laser duty cycle D. The latter is given by the ratio $D = \tau/\Delta t$, where τ is the pulse length and Δt is the time interval between two pulses given as $\Delta t = 1/f_{rep}$, which quantifies the overall temporal efficiency of the conducted experiment. The vast majority of LIBS experiments utilize flashlamp-pumped solid-state lasers, with repetition rates of 10 Hz and pulse lengths of approximately 10 ns

resulting in a duty cycle of $D = 10^{-7}$. These values, however, only represent the laser exposure duty cycle. Since laser-induced plasmas often have lifetimes of several microseconds, the duty cycle in terms of optical emission increases to 10^{-4}. Although in several publications an increase in LIBS response to materials with an increasing duty cycle has been observed, so far, no systematic reflection has been reported. Since an increase in the duty cycle can be achieved by an increase in the applied repetition rate or the use of longer laser pulses, the impact of both laser rate and pulse length determines the outcome of high duty-cycle LIBS.

Most studies in which high-repetition-rate lasers have been used in LIBS aimed either toward miniaturization and improved power management as can be found in diode-pumped solid-state (DPSS) Fabry–Pérot lasers [1–6] and fiber lasers [7–9] or toward superior sampling properties as observed in femtosecond laser applications [10–14]. In all reported results, different advantages were found compared to conventional 10-Hz flashlamp experiments although all mentioned laser sources provide much lower pulse energies. Generally, all observed beneficial effects of high repetition rates can be loosely summarized into three facets: i) improved statistics by a larger number of plasma events, ii) a weaker spectral background due to overall less energetic individual pulses, and iii) more moderate and temporally stable plasma conditions. The first benefit is the most straightforward, since all IR-laser–surface interactions rely on a multi-photon step for the initial generation of a seed electron and are, thus, prone to chance. Independently, several studies agree upon an increase in the signal-to-noise ratio (SNR) in the obtained results even for plasmas with a lower absolute brightness [3]. Another obvious advantage is the possibility to obtain full elemental information of samples within a shorter time. The latter is especially critical in sorting applications where spectrum-based decisions are made on a timescale governed by the sample feed.

The advantage of a lower background is caused by the internal plasma energetics. Distributing the same amount of energy that was introduced into the sample into several weaker pulses instead of one strong pulse has significant impact on the plasma-related background intensity. The amount of inverse bremsstrahlung and emission related to recombination, which is typical for early laser plasmas, dramatically decreases in laser pulses below a certain threshold pulse energy (typically several 1 mJ per pulse) [1–3, 8, 9]. This allows high repetition rates to gradually introduce large quantities of energy into the sample without increasing the amount of the spectrally broad background.

The overall lower excitation temperature observed in plasmas induced by weaker lasers can be advantageous. In recent years, the detection of molecular bands of rovibrational progressions of rovibronic transitions of residual diatomic species has gained popularity for the quantification of isotope ratios (via the so-called laser ablation molecular isotopic spectrometry or LAMIS [15]) or elements without elemental lines in the generally accessible UV/vis spectral region. In addition, low power lasers generally lead to a narrower temperature distribution (i.e., the smaller ΔT between an early and a late plasma), an effect which may be less straightforward but of equal importance for the analytical performance of LIBS experiments. Using low pulse energies results in significantly shorter lifetimes of the induced plasmas [3]. This shorter lifetime usually gets along with a temporally more homogeneous temperature distribution. On the other hand, the plasma lifetime is obviously of rising importance toward a duty cycle approaching unity since it dictates the rate at which the subsequent laser does not hit a thermally equilibrated target but arrives at a sample volume that is still excited by the previous plasma. This reheating of an existing plasma is known from double-pulse LIBS to greatly enhance the emission and improve the analytical performance in LIBS [16]. The residual energy in the system, until the subsequent laser pulse, does not need to be sufficient to maintain a plasma. In particular, LIBS experiments in dense media such as water were found to benefit from the residual energy from the previous plasma event, such as cavitation formed by a previous laser pulse [17–19].

The present study aims toward determining the beneficial effect of increasing the repetition rate and the temporal pulse width of laser pulses used in LIBS experiments. All experiments use a MOPA laser designed for engraving applications, allowing for freely adjusting both parameters in a wide parameter space. To systematically and comprehensively study the influence of the two parameters' length and rate, the optical responses of three individual spectroscopic contributions from a single Al alloy sample are being compared, namely, the Al matrix signal, the emission of Sr and Ca trace components, and the rovibronic progression of the diatomic AlO species.

2 Methodology

All experiments were carried out using the same master oscillator power amplifier (MOPA) fiber laser (JPT M7, 80 W, VONJAN Technology GmbH, Wessling, Germany) to provide laser pulses at λ = 1,064 nm with temporal widths between τ = 5 ns and τ = 500 ns at repetition rates ranging from $f_{rep.}$ = 1 kHz to $f_{rep.}$ = 1,550 kHz. Although the laser can produce even higher rates and shorter pulses, the corresponding pulse energies were found to be insufficient to obtain reasonable emission spectra. It is further worth noting that only combinations of rate and width resulting in laser peak powers approximately 8 kW or below are possible in order to not damage the internal laser fiber. The values for the pulse widths τ = 5, 10, 30, 40, 50, 60, 80, 100, 250, and 500 ns were chosen. The corresponding repetition rates dictated by the upper peak power limit mentioned previously result in $f_{rep.}$ = 40, 56, 140, 150, 180, 193, 210, 250, 612, and 1,550 kHz, respectively. For comparison, a set of experiments using the lowest possible repetition rate of 1 kHz was also added. A summary of all resulting combinations including the most important laser pulse parameters for the respective settings is given in Table 1.

A schematic of the experimental set-up is depicted in Figure 1. Briefly, the 7 mm (in diameter) output of the laser Faraday output coupler was directed on the dichroic IR-mirror of a confocal microscope assembly in which focusing of the laser onto an aluminum alloy target (AW-6082/3.2315) and collimation of the generated plasma emission are achieved by the same planoconvex fused silica lens (LA4148, Thorlabs, Bergkirchen, Germany) with f = 50 mm before the latter is refocused into an optical fiber by a surveillance camera lens (ACCF25123MP C-mount, AICO, Hangzhou, PR of China) with f = 25 mm and F = 1.2. The fiber delivers the collected light to the entrance slit of a Czerny–Turner

10.3389/fphy.2023.1241533

TABLE 1 Pulse parameters for the chosen laser setting.

(kHz)	5 ns	10 ns	30 ns	40 ns	50 ns	60 ns	80 ns	100 ns	250 ns	500 ns
1					Power/Watt					0.60
					Pulse energy/mJ					0.60
					Peak power/kW					1.20
40										70.00
										1.75
										3.50
56									70.00	70.00
									1.25	1.25
									5.00	2.50
140								68.00	70.00	70.00
								0.49	0.50	0.50
								4.86	2.00	1.00
150							63.00	70.00	70.00	70.00
							0.42	0.47	0.47	0.47
							5.25	4.67	1.87	0.93
180						63.00	70.00	70.00	70.00	70.00
						0.35	0.39	0.39	0.39	0.39
						5.83	4.86	3.89	1.56	0.78
193					62.00	70.00	70.00	70.00	70.00	70.00
					0.32	0.36	0.36	0.36	0.36	0.36
					6.42	6.04	4.53	3.63	1.45	0.73
210				64.00	68.00	70.00	70.00	70.00	70.00	70.00
				0.30	0.32	0.33	0.33	0.33	0.33	0.33
				7.62	6.48	5.56	4.17	3.33	1.33	0.67
250			60.00	69.00	70.00	70.00	70.00	70.00	70.00	70.00
			0.24	0.28	0.28	0.28	0.28	0.28	0.28	0.28
			8.00	6.90	5.60	4.67	3.50	2.80	1.12	0.56
612		50.00	70.00	70.00	70.00	70.00	70.00	70.00	70.00	70.00
		0.08	0.11	0.11	0.11	0.11	0.11	0.11	0.11	0.11
		8.17	3.81	2.86	2.29	1.91	1.43	1.14	0.46	0.23
1,550	60.00	70.00	70.00	70.00	70.00	70.00	70.00	70.00	70.00	70.00
	0.04	0.05	0.05	0.05	0.05	0.05	0.05	0.05	0.05	0.05
	7.74	4.52	1.51	1.13	0.90	0.75	0.56	0.45	0.18	0.09

spectrograph equipped with a charge-coupled device (CCD) imaging detector (Shamrock SR-303 i-B and iDus DU420A-BU, Andor Technologies, Belfast, Northern Ireland). The focal length and aperture of the spectrometer are 303 mm and F/4, respectively, and the spectral resolution with the low dispersing optical grating is 0.14 nm/pixel at the central wavelength of 458 nm. Dispersion via this 600 grooves/mm grating allows for simultaneous detection of a wavelength region from λ = 390 to 527 nm. In addition to characteristic lines, all spectra in these ungated experiments also include the optical background. The latter is understood here as the sum of all undesired signal contributions, i.e., everything not characteristic for an element or diatomic molecule. The main contribution is assumed to be blackbody radiation; however, minor contributions from recombination or bremsstrahlung and

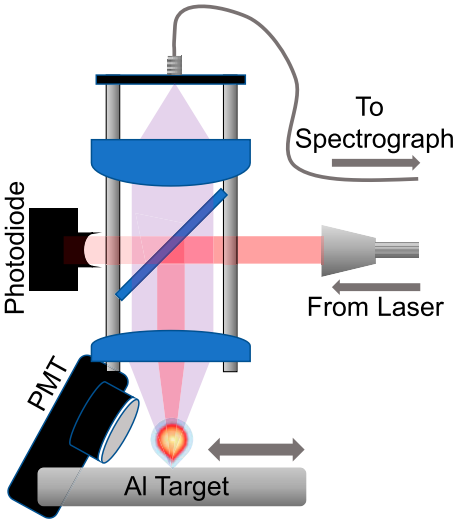

FIGURE 1
Schematic of the instrumental setup. Details are described in the text.

additional dark current can be superimposed. The extent of this background was quantified by recording the optical intensity at 460 nm, which lies close to the spectral center of the observation window but does not overlap with any spectral line of interest.

Synchronization of the laser output and the illumination and readout of the CCD was realized using two individual channels of a delay generator (DG645, Stanford Research Systems, Sunnyvale, United States). A fixed exposure time of 500 ms was used for all presented results during which the aluminum target was maintained in continuous motion to assure a fresh sample surface for all laser events. For an energetic characterization of the laser pulses, the output power of each combination of rate and width was determined using a pyroelectric power meter (Nova2, Ophir Spiricon, Darmstadt, Germany) and converted into the pulse energy and the pulse peak power (Table 1). For the temporal characterization of the laser pulses and the plasmas, a photodiode (PDA10A2, Thorlabs, Bergkirchen, Germany) was positioned behind the dichroic mirror to pick up the transmitted residual of the laser, while a photomultiplier tube (E717-63, Hamamatsu, Herrsching, Germany) was used to record the transient response of the plasma emission. Both signals were fed through 2-m-long coaxial cables and read out via two separate 50 Ohm terminated input channels of a WaveSurfer 4104HD oscilloscope (Teledyne LeCroy, Chestnut Ridge, United States).

3 Results and discussion

Before analyzing the impact of the laser duty cycle, pulse length, and repetition rate on the spectral response of the plasmas, the spectrally integrated temporal behavior of the plasma under different settings was analyzed. As an example for a typical transient signal of the laser and the corresponding plasma, Figure 2 shows the results for excitation with a laser pulse length of 250 ns at a rate of 56 kHz. As can be seen, the rising edge of the laser intensity is closely followed by the occurrence of plasma emission. Since both time traces were recorded simultaneously, the delay between the occurrences of two events can directly be extracted to be 20 ns. After this period, which it takes to form optically bright plasma, both signals reaches a maximum after which they decrease exponentially with the plasma response tailing the decay in the laser intensity in the decay starting time t_0. In addition to this delay of 60 ns, the exponential time constants of the two transients are also different. Although the laser intensity drops with a time constant of 50 ns, the decay of the plasma emission follows a slower kinetic with a $\tau_{exp.}$ of 270 ns. After the nominal pulse length of 250 ns, the laser emission stops in a steep decay, which is mirrored by a drop in the plasma emission intensity. The latter can be rationalized by the discontinuation of plasma reheating by the absorption of the irradiated infrared laser intensity. After the laser pulse, this steep decay in plasma emission is followed by an exponential tailing with a decay rate similar to that before the termination of the laser pulse. The extraction of the transient

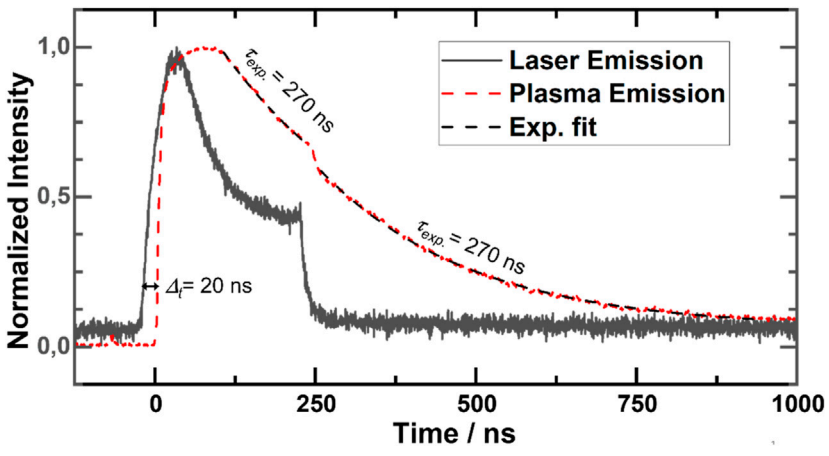

FIGURE 2
Typical temporal profile of the plasma inducing laser pulse and the plasma emission .

10.3389/fphy.2023.1241533

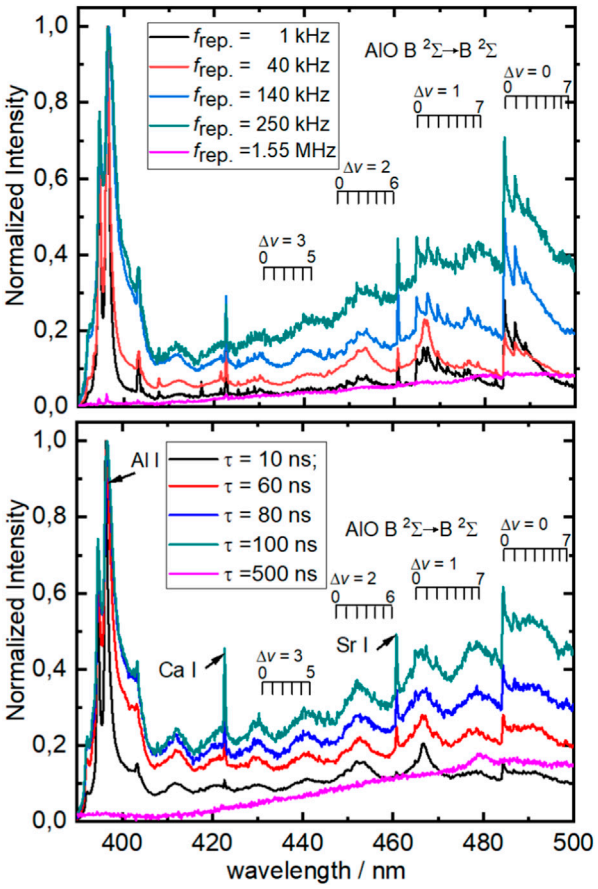

FIGURE 3
Exemplary LIBS spectra as a spectral response to repetition rates and temporal pulse widths. Top: Comparison between five different repetition rates (see legend) at the same pulse length (500 ns). Bottom: Comparison between five different pulse lengths (see legend) at a constant repetition rate (612 kHz) The spectra have been normalized for comparative visualization only.

parameters is exemplarily shown in Figure 2 and has accordingly been applied for all other studied laser pulse lengths resulting in comparable trends with exponential time constants between 200 and 400 ns. Toward shorter laser pulse lengths, the drop in plasma intensity toward the end of the laser pulse becomes deeper; at none of the studied combinations of repetition rate and pulse duration, a significant residual plasma emission at the time of the following laser pulse could be observed. In other words, none of the experiments presented here resemble the temporal arrangement usually applied in double-pulse experiments, in which a reheating of a preformed laser plasma is achieved via temporally overlaying the excitation decay and the subsequent laser pulse trigger.

Since no temporal overlap between the persisting plasma and the subsequent laser event could be observed, the repetition rate is not expected to affect the observed LIBS spectra drastically, and the most important factor in the remainder of this manuscript is considered to be the laser pulse duration. However, the studied combinations of rate and pulse length result in different laser energetics, which indirectly lets the rate reflect on the spectral performance. To get a comprehensive insight into both dependencies, LIBS spectra were recorded under all the aforementioned conditions. All individual combinations could be found to result in strikingly different spectral responses.

To lay a foundation for the detailed discussion of these differences and dependencies, Figure 3 exemplarily shows 10 LIBS spectra of the studied aluminum sample in the spectral range between 390 and 500 nm. Although aluminum can be considered a benchmark system for LIBS, since it has been at the core of a plethora of studies, the range was chosen because it contains the resonant elemental doublet corresponding to the relaxation of the first excited $^2S_{1/2}$ state into both spin–orbit components of the ^2P ground state and a rovibronic progression of the B $^2\Sigma \rightarrow$ X $^2\Sigma$ transition of the diatomic AlO systems [20, 21]. Two more spectral features in the range are the resonant lines of Ca I and Sr I at 422.7 and 460.7 nm, respectively.

As can be seen from the top graph shown in Figure 3, all laser settings led to the aforementioned spectral features. The most striking trends toward increasing repetition rates are a pronounced increase in the observed linewidth of the Al doublet as well as in a strong featureless peak introducing increasing background intensity toward the red end of the spectra. Although the latter can most likely be attributed to blackbody radiation caused by the thermal excitation of the solid target, the broadening can be rationalized by the self-absorption of the Al peak. Aluminum being the main component of the studied alloy and the transition being in resonance with the ground state, especially in the outer regions of the plasma, many potentially absorbing Al atoms can be expected. Since the broadening increases toward higher rates, it can be argued whether these cold Al atoms were formed in the current laser event or the previous laser event and persist accordingly over the period between two subsequent pulses. In the rates depicted in the upper trace of Figure 3, these inter-pulse intervals decrease with the increasing rate, and the interval durations are 1 ms, 25 µs, 7 µs, 4 µs, and 645 ns. At the rate of 1.5 MHz, the energy of the individual laser pulses appears to be insufficient to induce enough ablation of Al, and the same can, however, be observed for all spectral features in the spectrum. The lower trace of Figure 3 shows the same broadening to occur at a fixed repetition rate upon increasing pulse duration.

The presence of a strong and resolved molecular band is surprising in this non-gated experiment since diatomic band structures are usually reported in the late and cold stages of experiments with a delayed spectral acquisition. With the increasing repetition rate, the intensity of the bands increases until at the highest rate where apparently no spectral information can be observed. Similar to the broadening of the Al I line, the lower trace reveals the intensity of the diatomic bands to also increase toward longer pulse durations at a fixed laser excitation rate. In addition, the intensity of the Sr and Ca lines appears to scale with the laser rate and pulse length in a similar way.

In this way, the elemental line intensities of Al, Ca, and Sr can be directly related to the plasma formation efficiency, while the presence of molecular bands can be interpreted as an internal thermometer. Typically being observed in late plasmas which have been cooled down via collisional and radiative heat dissipation, molecular bands are spectrally structured, weak, and their statistically significant detection requires long accumulation times. Since one of the goals of this work is to showcase a simple and

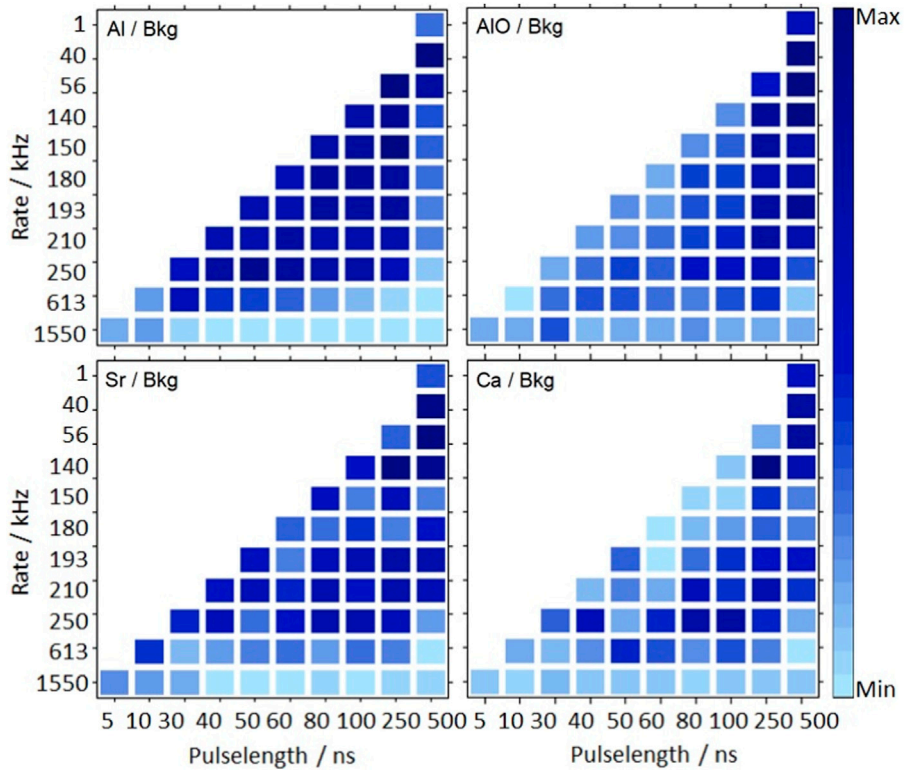

FIGURE 4
Heatmap of the background-corrected optical response of the signal intensity of the elemental lines of Al (top left), Sr (bottom left), and Ca (bottom right), as well as the R1 bandhead of the Δv = 0 progression of the B→X transition of AlO. All signal intensities are plotted over the repetition rate and the pulse length of the used excitation laser.

inexpensive yet powerful LIBS setup, molecular band intensity was included in the features of interest. In addition to the intensity of the Al doublet I_{Al} and the rovibrational bandhead of the $\Delta v = 0$ band I_{AlO}, the spectral background is also of paramount importance since it dictates the applicability of non-gated detectors. Here, the term background is generally understood as undesired intensity in the spectra. A distinction between the electronic background like readout noise and optical background is not being made. As has been discussed, most of the unwanted optical signal stems from blackbody radiation and, thus, scales with the wavelength. For this reason, a common value was determined as the spectral intensity at 460 nm, which is close to the spectral center wavelength and outside any characteristic emission carrying chemical information. For a more comprehensive and systematic analysis of the discussed trends, the individual intensities of the five aforementioned features in all spectra were extracted as the non-normalized intensities at $\lambda = 396.6$, 422.7, 460, 460.7, and 484.4 nm representing the spectral contribution of Al, Ca, an average value for the blackbody radiation, Sr, and AlO, respectively. For the quantification of the blackbody background, the single value of $I_{(460\ nm)}$ was chosen due to its central position in the spectrum and the absence of any spectral features in this spectral region. All other spectral intensities in the remainder of this manuscript are given as a ratio of the respective spectral intensity observed in the raw spectrum to the spectral intensity at this reference point in the same spectrum $I_{(x)}/I_{(460\ nm)}$.

An overview of the obtained background-corrected intensities as a function of the repetition rate and pulse length is presented as four heatmaps in Figure 4. All four signal intensities can be found to strongly depend on both rate and length of the used laser pulses; however, the exact dependencies differ.

The intensity of the Al line at $\lambda = 396$ nm is the highest in the range between a rate of 40 kHz and 250 kHz and pulse lengths of 30 and 250 ns. Above this, at rates of 612 kHz and pulse durations of 500 ns, intensity is still moderate, while beyond these values, the signal drops significantly. Within the optimum region, hardly any variation can be observed, indicating a very robust signal response of both the Al line intensity and the integrated spectral background (note: the value plotted here is the ratio of the two). This can be explained by the strong self-absorption behavior already shown in Figure 3 and the generally low background signal intensity. Although the self-absorption leads to a saturated and, thus, constant peak intensity, the small background maintains this small variance in the signal-to-background (S/B) ratio. In this sense and considering Al being the main component of the alloy, the decrease in the Al/Bkg intensity toward the edges plotted in Figure 4 directly indicates a decrease in the overall elemental plasma emission at rates exceeding 250 kHz and widths above 250 ns. A comparison of the individual laser pulse energetics in Table 1 suggests an interplay between a drop in the pulse energy and the number of events to cause this decrease.

Interestingly, the maximum intensity in the molecular progression of the B-band of AlO is observed under distinctively different conditions. This spectral feature, which is usually observed at lower plasma temperatures, peaks toward longer pulses and shows its maximum at τ = 500 ns. Within the group of spectra with this pulse length, the AlO/Bkg intensity decreases with the increasing repetition rate. The latter can again be caused by the corresponding drop in the pulse energy, leading to insufficient plasma excitation or unfavorable ablation behavior. The moiety of long pulses, which is beneficial for molecular bands while at the same time being detrimental for the strong elemental line of the major component, can be of special interest for LAMIS studies. These laser settings in a LAMIS application would allow for optical isotope analysis with an affordable laser in combination with an inexpensive non-gated detector scheme.

Both trace alloy components, Ca and Sr, finally, also exhibit characteristic regions of maximum elemental emission. The two distributions Ca/Bkg and Sr/Bkg in the heatmaps in Figure 4 differ strongly from each other, with the Ca signal peaking at laser settings similar to the appearance of the maximum AlO while Sr bears a closer resemblance to the behavior of the Al line. Energetically, this is unexpected because both transitions are resonant with the respective element in its electronic ground state, with the individual upper state electronic energies only differing in ~2,000 cm^{-1} (0.25 eV). These similar excitation energetics indicate that the cause for the different abundances in the heatmaps is more likely due to phase transition properties, leading to individual laser ablation characteristics.

4 Conclusion

The application of a MOPA laser for LIBS allows for an increased flexibility in laser pulse characteristics. Although conventional Fabry–Pérot cavity-based lasers only allow for a variation in the pulse energy and are operated at very low duty-cycles, an MOPA operates on the other end of the duty spectrum and additionally introduces repetition rate and pulse length as two variable pulse characteristics. A comprehensive study of the temporal plasma behavior shows the strong impact of the pulse length on the plasma dynamics. The transient plasma emission was found to closely follow the excitation laser pulse shape. The variations in both rate and length were found to strongly affect the spectral response of an aluminum sample. Although the spectral emission intensity of elemental lines of the three different species, Al, Sr, and Ca, could be found to depend differently on these parameters, the relative intensity of molecular bands of diatomic AlO was particularly found to peak at distinct laser settings. The latter is of special interest since it may pave the road toward future isotope analysis studies with sensitive and flexible yet inexpensive and robust instrumentation.

Data availability statement

The raw data supporting the conclusion of this article will be made available by the authors, without undue reservation.

Author contributions

YY and JR jointly conceived the idea of the experiment. JH conducted the experiment. YY and JH analyzed and visualized the results. JR supervised the project and drafted the manuscript. Based on this first draft, all authors jointly reviewed the manuscript. All authors contributed to the article and approved the submitted version.

Acknowledgments

The authors are indebted to Igor B. Gornushkin for fruitful discussion on the underlying plasma dynamics and the spectral assignment.

Conflict of interest

The authors declare that the research was conducted in the absence of any commercial or financial relationships that could be construed as a potential conflict of interest.

Publisher's note

References

1. Amponsah-Manager K, Omenetto N, Smith BW, Gornushkin IB, Winefordner JD. Microchip laser ablation of metals: Investigation of the ablation process in view of its application to laser-induced breakdown spectroscopy. *J Anal At Spectrom* (2005) 20(6): 544–51. doi:10.1039/b419109a

2. Freedman A, Iannarilli FJ, Wormhoudt JC. Aluminum alloy analysis using microchip-laser induced breakdown spectroscopy. *Spectrochimica Acta B: At Spectrosc* (2005) 60(7):1076–82. doi:10.1016/j.sab.2005.03.020

3. Gornushkin IB, Amponsah-Manager K, Smith BW, Omenetto N, Winefordner JD. Microchip laser-induced breakdown spectroscopy: A preliminary feasibility investigation. *Appl Spectrosc* (2004) 58(7):762–9. doi:10.1366/0003702041389427

4. Lopez-Moreno C, Amponsah-Manager K, Smith BW, Gornushkin IB, Omenetto N, Palanco S, et al. Quantitative analysis of low-alloy steel by microchip laser induced breakdown spectroscopy. *J Anal At Spectrom* (2005) 20(6):552–6. doi:10.1039/b419173k

5. Wormhoudt J, Iannarilli FJ, Jones S, Annen KD, Freedman A. Determination of carbon in steel by laser-induced breakdown spectroscopy using a microchip laser and miniature spectrometer. *Appl Spectrosc* (2005) 59(9):1098–102. doi:10.1366/0003702055012528

6. Pořízka P, Klessen B, Kaiser J, Gornushkin I, Panne U, Riedel J. High repetition rate laser-induced breakdown spectroscopy using acousto-optically gated detection. *Rev Sci Instrum* (2014) 85(7):073104. doi:10.1063/1.4890337

7. Bohling C, Hohmann K, Scheel D, Bauer C, Schippers W, Burgmeier J, et al. All-fiber-coupled laser-induced breakdown spectroscopy sensor for hazardous materials analysis. *Spectrochimica Acta Part B: At Spectrosc* (2007) 62(12):1519–27. doi:10.1016/j.sab.2007.10.038

8. Gravel J-FY, Doucet FR, Bouchard P, Sabsabi M. Evaluation of a compact high power pulsed fiber laser source for laser-induced breakdown spectroscopy. *J Anal At Spectrom* (2011) 26(7):1354–61. doi:10.1039/c0ja00228c

9. Scharun M, Fricke-Begemann C, Noll R. Laser-induced breakdown spectroscopy with multi-kHz fibre laser for mobile metal analysis tasks — a comparison of different analysis methods and with a mobile spark-discharge optical emission spectroscopy apparatus. *Spectrochimica Acta Part B: At Spectrosc* (2013) 87:198–207. doi:10.1016/j.sab.2013.05.007

10. Baudelet M, Guyon L, Yu J, Wolf JP, Amodeo T, Frejafon E, et al. Femtosecond time-resolved laser-induced breakdown spectroscopy for detection and identification of bacteria: A comparison to the nanosecond regime. *J Appl Phys* (2006) 99. doi:10.1063/1.21871078).

11. Bordel N, Fernandez-Menendez LJ, Mendez-Lopez C, Gonzalez-Gago C, Pisonero J. Halides formation dynamics in nanosecond and femtosecond laser-induced breakdown spectroscopy. *Plasma Phys Controlled Fusion* (2022) 64, 054010. doi:10.1088/1361-6587/ac5c115).

12. Chen YT, Liu YT, Wang QY, Li SY, Jiang YF, Chen AM, et al. Effect of laser polarization on molecular emission from femtosecond LIBS. *J Anal At Spectrom* (2022) 37(1):82–8. doi:10.1039/d1ja00308a

13. Labutin TA, Lednev VN, Ilyin AA, Popov AM. Femtosecond laser-induced breakdown spectroscopy. *J Anal At Spectrom* (2016) 31(1):90–118. doi:10.1039/c5ja00301f

14. Le Drogoff B, Margot J, Chaker M, Sabsabi M, Barthelemy O, Johnston TW, et al. Temporal characterization of femtosecond laser pulses induced plasma for spectrochemical analysis of aluminum alloys. *Spectrochimica Acta B-Atomic Spectrosc* (2001) 56(6):987–1002. doi:10.1016/s0584-8547(01)00187-2

15. Bol'shakov AA, Mao XL, Gonzalez JJ, Russo RE. Laser ablation molecular isotopic spectrometry (LAMIS): Current state of the art. *J Anal At Spectrom* (2016) 31(1):119–34. doi:10.1039/c5ja00310e

16. Babushok VI, DeLucia FC, Gottfried JL, Munson CA, Miziolek AW. Double pulse laser ablation and plasma: Laser induced breakdown spectroscopy signal enhancement. *Spectrochimica Acta Part B-Atomic Spectrosc* (2006) 61(9):999–1014. doi:10.1016/j.sab.2006.09.003

17. De Giacomo A, Dell'Aglio M, De Pascale O, Capitelli M. From single pulse to double pulse ns-Laser Induced Breakdown Spectroscopy under water: Elemental analysis of aqueous solutions and submerged solid samples. *Spectrochimica Acta Part B-Atomic Spectrosc* (2007) 62(8):721–38. doi:10.1016/j.sab.2007.06.008

18. Xue BY, You Y, Gornushkin I, Zheng R, Riedel J. High-throughput underwater elemental analysis by mu J-laser-induced breakdown spectroscopy at kHz repetition rates: Part I, ultrasound-enhanced optical emission spectroscopy towards application perspectives. *J Anal At Spectrom* (2020) 35(12):2901–11. doi:10.1039/d0ja00290a

19. Xue BY, You Y, Riedel J. High-throughput underwater elemental analysis by mu J-laser-induced breakdown spectroscopy at a kHz repetition rate: Part II, understanding the high repetition-rate from a fundamental perspective. *J Anal At Spectrom* (2020) 35(12):2912–9. doi:10.1039/d0ja00291g

20. Bowesman C, Shuai M, Yurchenko S, Tennyson J. *A high-resolution line list for AlO* (2021). doi:10.1093/mnras/stab2525

21. Bowesman C. A., Shuai M., Yurchenko S. N., Tennyson J. A high-resolution line list for AlO. *Monthly Notices of the Royal Astronomical Society* (2021) 508(3):3181–3193. 10.1093/mnras/stab2525.